Sustainable Energy & Fuels

ROYAL SOCIETY OF CHEMISTRY

PAPER

View Article Online
View Journal | View Issue

Cite this: *Sustainable Energy Fuels*, 2023, 7, 461

A framework for comparing the energy production of photovoltaic modules using 2-, 3-, and 4-terminal tandem cells†

William E. McMahon, *[a] John F. Geisz, [a] Jeronimo Buencuerpo [abc] and Emily L. Warren [a]

One of the design choices to be made when constructing photovoltaic modules from tandem solar cells is whether to use 2-, 3-, or 4-terminal tandem devices. Two-terminal (2T) cells are the simplest to interconnect, but for effective energy production the two subcells must be current-matched, which constrains the choice of materials for the component subcells. Three-terminal (3T) cells can be interconnected in voltage-matched configurations, which greatly increases the number of suitable subcell bandgap combinations, but with some additional cell interconnection complexity and losses. In principle, four-terminal (4T) cells provide the best power production, but in practice this will be mitigated by losses associated with the more complex interconnection requirements and shading losses necessitated by the need to laterally transport carriers between the cells. Many comparisons have been made between 2T and 4T configurations, mostly at the cell level. Here we provide a framework to assess the relative performance of 3T voltage-matched configurations relative to 2T and 4T approaches at the module level. We compare the energy production for both a fixed standard spectrum, and under variable outdoor conditions (accounting for spectrum, temperature, and location). The methods presented enable the comprehensive visualization and comparison of string-end losses, voltage matching ratios, and resistive and optical losses for tandems constructed out of any solar cell materials.

Received 26th August 2022
Accepted 2nd December 2022

DOI: 10.1039/d2se01167k

rsc.li/sustainable-energy

Introduction

Tandem solar cells can outperform single-junction cells in both cell efficiency and energy production, making them a promising approach for the next generation of photovoltaic modules.[1–4] Recent advances at the cell level have demonstrated one sun efficiencies that exceed the detailed balance limit for single junction solar cells, using a variety of material combinations including perovskite/Si[5] and III–Vs.[6] Here we consider one aspect of tandem cell design that introduces both challenges and opportunities: the number of external terminals to the cell. Using representative two-junction solar cells contacted by 2, 3, or 4 terminals, (abbreviated 2T, 3T, and 4T, respectively and shown schematically in Fig. 1), we illustrate the fundamental points and limiting cases for different cell-level terminal configurations.

Each terminal configuration has different performance under varying spectral and thermal conditions, so comparing the total power produced over a given time period is necessary to compare the relative merits of 2T, 3T, and 4T configurations, and guide design decisions. Here we use Energy Harvesting Efficiency (EHE) as a metric for the modeled performance of solar cells under varying spectra and conditions representative of outdoor operation, where EHE refers to the energy produced

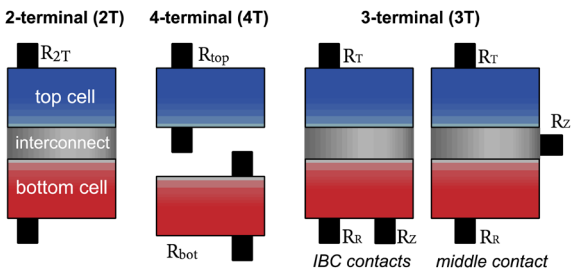

Fig. 1 Schematics of 2T, 4T, and 3T tandem cells illustrating the different contacting arrangements for each. For 2T, all series resistance is typically lumped into a single value. For 4T, two R_{series} values are used, one for the top cell, and another for the bottom cell. A 3T cell requires three independent resistances (one for each contact: R_T, R_Z and R_R).

[a]National Renewable Energy Laboratory, Golden, CO, USA. E-mail: bill.mcmahon@nrel.gov
[b]L'Institut Photovoltaïque d'Île-de-France (IPVF), Palaiseau, France
[c]Centre de Nanosciences and Nanotechnologies (C2N), CNRS, Paris-Saclay University, Palaiseau, France

† Electronic supplementary information (ESI) available. See DOI: https://doi.org/10.1039/d2se01167k

by a string of tandem cells divided by the incident solar energy during the same timespan (in this work, one year).

A 4T tandem cell can be connected to two loads such that each subcell always operates at its maximum power point (mpp). In principle this maximizes energy production, but it also requires additional current collection and isolation layers which decrease performance. A 2T tandem cell is in many ways the simplest configuration, but its series-connected configuration constrains the choice of subcell materials to those which are current-matched, and makes it sensitive to variations in the spectral content of the incident light.

A 3T configuration is an intermediate case. 3T tandems cells have been demonstrated experimentally[7–9] and simulations show that they can have efficiencies similar to 4T tandems if designed properly.[10,11] A 2T module formed from 3T tandem cells places the subcells in a voltage-matched state, which reduces spectral sensitivity and relaxes the constraints on subcell choices. However, the associated cell-stringing complexity must be understood and included as part of any comparison with 2T and 4T configurations.

Numerous EHE studies have compared the relative merits of 2T and 4T tandem cells,[10,12–14] but studies which include 3T tandem cells are less common.[10] The EHE modeling presented here builds upon prior work to include 2T modules constructed from voltage-matched strings of 3T tandem cells, using representative examples of different bandgap combinations. This framework provides a way to directly compare how tandems integrated with different terminal configurations will perform in real world scenarios.

The fundamentals of voltage-matched (VM) strings formed from 3T tandems have been described by McMahon *et al.*[15] (and references therein). This prior work showed how 2T strings can be created from 3T tandems using different subcell voltage-matching ratios (V_{top}/V_{bot}), and described the associated string-end losses. (These losses are independent of string length, hence minimized for longer strings). Here we add this fundamental understanding to EHE calculations under varying spectra representative of a particular location.

This analysis includes the string-end losses and voltage-matching constraints inherent to VM strings, both of which are neglected for an EHE calculation in which a single 3T cell is connected to two independent loads.[10] We also illustrate how series-resistance considerations for 3T tandems differ from the 2T and 4T configurations.

The goal of this paper is to illustrate a method for visualizing and comparing the numerous design tradeoffs between 2T, 3T, and 4T tandems. To accomplish this, it is helpful to plot all results as a function of string length, which impacts 3T design decisions due to string-end loss (but not 2T or 4T designs). Results are shown for both EHE in Boulder, CO, and power-conversion efficiency under the standard AM1.5G spectrum. Similar qualitative behavior is seen for both, demonstrating that for many design decisions the use of a single design spectrum (like AM1.5G) can provide considerable insight.

These methods will be illustrated with representative tandem III–V and Si cells, but they are equally applicable to subcells made from any material (*e.g.* perovskites), using any set of spectra. Realistic modeled IV parameters based on recent literature measurements were chosen for their utility as example cells for the purposes of illustration.

It should be emphasized that the example comparisons used in this paper are idealized so as to focus on electrical losses inherent to 2T, 3T, and 4T designs. The relative performance of any given set of tandem cells will, of course, also be greatly affected by additional "real-world" losses specific to their designs.

Most significantly, losses related to optical transmission through the top cell have been neglected in all examples, so as to focus on other effects. The impact of optical losses on device performance has been studied previously.[16,17] If (for example) these losses affect 4T cells more than 2T or 3T cells, then the relative performance in any comparison will need to be adjusted accordingly. Studies investigating optical transmission losses require careful analysis specific to the exact tandem cell architecture being considered; examples of this can be found elsewhere.[18–21]

It is also worth noting that the quality of the subcells used in a tandem cell impacts any performance comparison of 2T, 3T, and 4T devices, so the conclusions drawn from the examples shown here are very specific to the subcells used. The methods shown here are completely material agnostic, and can be applied to any set of subcells to reach conclusions for any subcell combination of interest, including all associated losses. (For example, subcell bandgaps are often adjusted in a 2T tandem to attain current-matching, and this type of bandgap adjustment can be done within the framework described here.)

Background and nomenclature

The tandem cell configurations modeled in this study are shown in Fig. 1. The performance of these devices is modeled using equivalent circuits that utilize parameters which can be fit for any subcell material (Fig. S1†), making the methods equally applicable to a wide variety of cell architectures and materials. For example, the interconnect used for the 2T configuration could be a tunnel junction or an electrically conductive mechanical bond. In either case the equivalent circuit would parameterize this or any analogous interconnect with a series resistance, and any optical-transmission loss through the interconnect would reduce the bottom-cell external quantum efficiency (EQE).

The equivalent optoelectronic circuits used to model 2T, 3T, and 4T tandem solar cells are described in detail elsewhere.[22–24] Here the resistances are treated in the most rudimentary fashion. In a 2T device, all series resistances are combined into a single R_{series} value "R_{2T}". In a 4T device, the top and bottom subcells each have their own series resistance (R_{top} and R_{bot}) which includes the resistance of the additional contacts. For 3T devices, each contact has its own series resistance (R_T, R_Z and R_R).

These resistive losses can be important but will be set to zero for the main part of this paper in order to clearly illustrate and compare non-resistive losses for different cell configurations. For 2T tandems, it is important to understand power loss due to

current-mismatch and spectral variation. A 3T tandem is less sensitive to spectral variation, but voltage-matched strings created from 3T tandems have string-end and voltage-matching losses. With resistive losses neglected, a 4T tandem provides an upper performance limit for these comparisons. Once these non-resistive losses have been fully illustrated, resistive and optical losses will be reintroduced for a more complete comparison.

To discuss current-mismatch and spectral variation in 2T tandems, it is helpful to first define some associated nomenclature. The term "current matched" means that the subcells have the same short circuit current (I_{sc}, which, to an excellent approximation, gives them the same maximum power point current, I_{mpp}). Current-matching significantly impacts the performance of 2T cells. If a 2T cell is perfectly current-matched, both subcells can simultaneously operate at their respective maximum power points (mpps). When the subcells are not current-matched for a given spectrum, the current of a 2T tandem cell is limited by the lower of the two subcell currents, reducing the power production accordingly.[25,26]

Spectral variation refers to the fact that the outdoor solar spectrum is constantly changing, which creates varying amounts of current-mismatch in a 2T device. This makes it impossible for the component subcells to always operate at their respective mpps, which reduces the energy production of a 2T tandem.[10,27,28] (In contrast, a 4T tandem can be connected to two loads such that both subcells can always operate at their respective mpps. For this reason, an ideal 4T tandem serves as an upper limit for performance if resistive and optical losses are neglected.)

A 3T configuration has a reduced sensitivity to spectral variation and some other potential advantages, but also introduces some additional complexity.[10,11] Most obviously, there are three contacts: A "T" contact at the top, an "R" contact at the rear, and an additional "Z" contact between the subcells.[29] (If an interdigitated back-contact bottom cell is used, the Z contact shifts to the bottom of the IBC cell as shown in Fig. 1, eliminating the need for a lateral-conduction layer or grid between the subcells.)

The third (Z) contact can also eliminate the need for a tunnel junction between the subcells, if an "r-type" connection is used. This places the subcells in a "back-to-back" configuration with their diode senses reversed (Fig. 2b). If the two component subcells are configured in series (s-type connection), then a tunnel junction or similar interconnection is needed (Fig. 2a). Note that the magnitude of the I_Z current is different for the two configurations due to the reversed diode directions for r-type (additive subcell currents) and the same diode direction for s-type (subtractive subcell currents). One consequence of this is that the $I_Z^2R_Z$ losses will be greater for r-type devices, all else being equal.

When 3T cells are connected together to form a VM string, the interconnection configuration between the component tandem cells establishes a voltage-matching ratio $V_{top}/V_{bot} = m/n$ (where m and n are integers).[15] If the VM ratio is 2/1, for example, each top cell will be wired in parallel with two series-connected bottom cells, establishing a 2/1 VM ratio. (For a 3/2 ratio, two series-connected top cells will be wired in parallel with three series-connected bottom cells.)

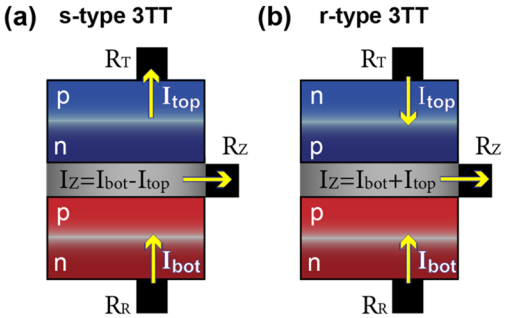

Fig. 2 (a) Two series-connected subcells (s-type tandem), for which the doping sequence (p/n) is the same for both subcells. (b) Two reverse-connected subcells (r-type tandem), for which the doping sequence of the two subcells are reversed with respect to one another. (Equivalent circuits are shown in Fig. S1c and d.†)

For best performance of a VM string, each subcell should be operated near its respective V_{mpp}, so the best VM ratio will be near the ratio of V_{mpp}(top)/V_{mpp}(bot). This could be advantageous, because it would enable the use of subcell bandgap combinations which are unsuitable for 2T current-matched tandem cells, without some of the optical and electrical losses often associated with 4T configurations (*i.e.* related to the placement of low-index dielectrics and grids or heavily doped laterally conductive layers between the subcells of a 4T tandem). However, all VM strings formed from VM tandem cells have an inherent end-of-string loss[15] which is particularly important for short strings, and must therefore be properly accounted for. (As will be seen, this loss becomes negligible for long strings.) One possible weakness of a voltage-matched configuration might be sensitivity to temperature variations, because the ratio of the subcell V_{mpp} values (measured independently) can change logarithmically with temperature, altering the ideal VM ratio.

Methods

The location chosen for the examples in this study was a site near Boulder Colorado, USA, (latitude 40.31°, longitude 105.22°), and the spectra used were for a single-axis tracking configuration with front-side illumination only. Whereas many studies use very large sets of spectra (*i.e.* hourly spectra over the course of a year), this study used a much smaller set of just 18 "proxy" spectra generated by machine learning methods,[24,28,30] using multijunction performance as a training metric to ensure computational accuracy is maintained.

The use of a small proxy set has two main benefits. The most obvious is that it eliminates the need to compute the cell performance for numerous nearly identical spectra, making calculations more computationally efficient. A second, less obvious benefit is that grouping together spectra with similar irradiance and spectral content facilitates visualization and understanding. This makes it clear, for example, that most of the incident solar energy arrives during the middle of the day, when the spectra are quite similar.

Cell performance calculations used optoelectronic equivalent-circuit models which includes luminescent coupling (LC) from the top subcell to the bottom subcell (Fig. S1†).[22–24] Luminescent coupling effects are important to consider for a tandem solar cell, especially when it is operated at non-optimal conditions such as over-illuminated top-subcell conditions. A two-diode model for each subcell is used here. The temperature dependence of the reverse-saturation current of each subcell in the model is relative to the detailed-balance saturation current (J_{db}) as described in the ESI.†

To populate these equations with the parameters needed for cell modeling, representative 3T tandem cells previously described in the literature were measured using the methods from Geisz *et al.*[23] To illustrate the inherent differences between 2T, 3T, and 4T configurations, the same diode parameters were used for all three configurations. In reality, the characteristics of diodes in these different configurations are likely to be different, but these differences are highly situational and outside the scope of this paper. However, one important detail common to all tandem cells is that the top subcell must allow transmission of light to the bottom cell. Using cell parameters for a top subcell with a fully metallized back contact can lead to overly optimistic estimations and provides no information about how much bottom cell light it would attenuate if used as part of a tandem cell. The results presented here utilized parameters extracted from tandem cells, using the requisite transparent top cells. Information about how these parameters were extracted from cell measurements is provided in the ESI.†

The overall flowchart for the EHE calculations is shown in Fig. 3. Within this framework, the calculation of a tandem cell efficiency under a given spectrum (*i.e.* AM1.5G) is done in four steps: (1) the subcell EQEs are convolved with the incident spectrum to compute subcell photocurrents, (2) the tandem cell power is computed using the equivalent-circuit model using these photocurrents as current sources for the subcells, (3) adjustments are made for the string-end losses inherent to VM strings, and (4) the resulting power is divided by the irradiance of the incident spectrum.

An EHE computation performs the above steps for each of the spectra in a set of spectra, then averages the resulting efficiencies weighted by a time associated with each spectrum. Often the time associated with each spectrum is the same (*i.e.*, one hour), and all spectra are weighted equally. However it is also possible for the time associated with each spectrum to be different. This typically happens when spectra are combined into a reduced set of "proxy" spectra, as was done for the source spectra used in this paper. The environmental factors associated with each spectrum (*i.e.*, ambient temperature and wind speed) can also vary, such that the solar cell temperature for each spectrum is different. The cell temperature was held at 25 °C for the standard AM1.5G spectrum, but calculated from environmental factors (*i.e.* ambient temperature and wind speed) for each proxy spectrum using the Sandia model.[31]

The performance of modules of 2T cells are calculated as the performance of a 2T cell under a single load. The performance of modules of 4T cells are determined as the performance of 4T cells operated under two independent loads (though this may not be economically viable). The performance of modules of 3T cells are determined assuming series-parallel "voltage-matched" strings as described by McMahon *et al.*[15] operating under a single 2T load that results in end-losses. The 3T calculations are done for both s- and r-type tandems, with different candidate VM ratios and string lengths. The maximum 3T cell performance is calculated under voltage-constrained conditions and the module end-losses are applied as:

$$P_{\text{endloss}} \approx \begin{cases} (m+n-1) \times P_{\text{tandem}} & \text{for s-type} \\ [\max(m,n)-1] \times P_{\text{tandem}} & \text{for r-type} \end{cases}$$

where m bottom subcells are strung in parallel to n top cells, P_{endloss} is the power loss for the string related to end losses, and P_{tandem} is the power of a single tandem cell.

Results

The results shown here illustrate the relative merits of 2T, 3T, and 4T configurations under different circumstances using representative tandem cell examples. The goal of this study is to illustrate methods which are equally applicable to any subcell material combination, so the example cells used in this paper were chosen primarily for their illustrative value because they have moderate efficiency and high stability, enabling reproducible experimental measurements.

Our first comparison is based upon a current matched ("CM") tandem example comprised of current-matched subcells well-suited for a 2T configuration (GaInP and Si subcells). The second example is a "VM Tandem" with subcells more appropriate to a voltage-matched configuration (GaAs and Si subcells). A third "Generic Tandem" example illustrates some of the inherent design compromises between these two extremes (GaInP and GaAs subcells).

For these first three examples, all series resistances and optical losses external to the subcells are neglected to clearly delineate differences due to spectral mismatch and spectral variability. After these have been described in detail, a final example illustrates the impact of resistive losses, and optical losses are discussed. Because the same basic equivalent circuit can parameterize any well-designed solar cell, the methods and

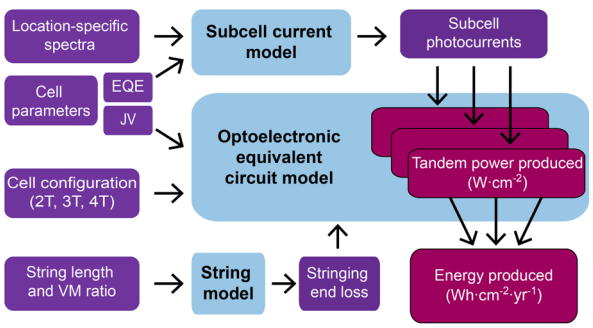

Fig. 3 Flowchart illustrating the EHE computational methods used in this paper.

basic results are extensible to a wide variety of cell materials and architectures.

Current-matched tandem

Fig. 4 and 5 show results for a "CM Tandem" case in which the subcells are nearly current-matched. An s-type GaInP/Si 3T tandem cell that we have previously published was chosen as the basis for this example.[32] Because the EQE of the Si cell is a little low, this example is not an assessment of the upper limits of GaInP/Si performance. Instead, it is included because it serves as an excellent example of a nearly current-matched (CM) tandem cell. The measured EQE of this CM tandem is shown in Fig. 4a and the modeled diode parameters fit to the data are given in Fig. S2a.† Subcell *JV* curves for this example calculated under the AM1.5G spectrum at 25 °C are shown as green lines in Fig. S3.† The same subcell diode parameters were used for calculations of 2T, 3T, and 4T performance.

Because 2T tandems are sensitive to photocurrent mismatches between the subcells, it is instructive to plot the two subcell photocurrent values corresponding to each spectrum, as is done in Fig. 4b. (Fig. S4 and S5† indicate the temperature and fractional time corresponding to each spectrum, respectively). This plot contains 18 points, one for each spectrum in a set of "proxy" spectra representing a full year at a site near Boulder, Colorado, USA. The position of each spot is given by the subcell photocurrents generated under each spectrum. The distance from the origin is therefore related to each spectrum's irradiance, whereas the distance from the current-matched line is related to current mismatch, which can be different for each spectrum due to spectral variation.

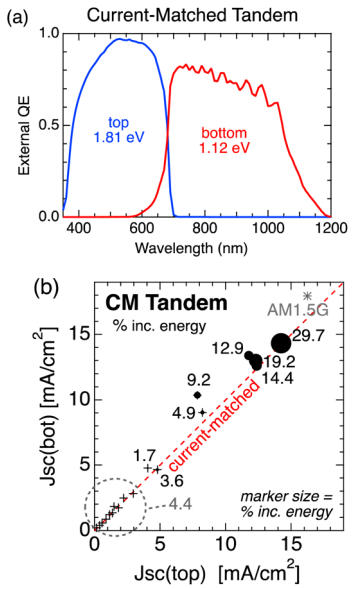

Fig. 4 (a) External quantum efficiency of the current-matched "CM" tandem example cell based upon a GaInP/Si tandem cell. The *JV* model parameters are listed in Fig. S2a,† but resistive and optical shadow losses are omitted. (b) Photocurrent densities of bottom *versus* top subcells produced by the CM tandem cell under each spectrum in a set of spectra used for EHE calculations. The size of each point here represents the fraction of incident energy corresponding to that spectrum, with "+" markers indicating the positions of the smaller points. The encircled cluster of spectra in the lower left represents just 4.4% of the incident energy. A grayed point indicating the subcell photocurrent densities under the AM1.5G reference spectrum is included for comparison.

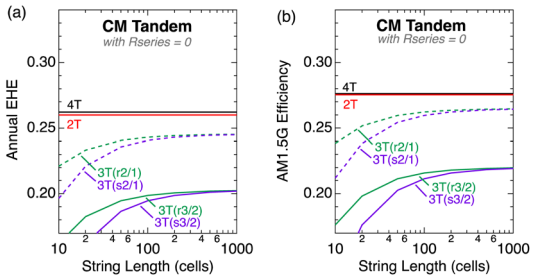

Fig. 5 Cell performance results for a representative current-matched (CM) tandem from Fig. 4. (a) Energy-harvesting efficiency and (b) conversion efficiency under the AM1.5G spectrum for 2T, 3T, and 4T tandems. The 3T curves have been labeled "r *m*/*n*" and "s *m*/*n*", to indicate r- and s-type, respectively, with two representative voltage-matching ratios *m*/*n* of 2/1 and 3/2. Note: All series resistances and optical transmission losses have been set to zero to clearly delineate other effects.

If hourly spectra had been used, these plots would have contained several thousand points. Here, similar spectra have been grouped together by a machine-learning algorithm.[28,30] This facilitates visualization of both the current mismatch and spectral variability for any given tandem cell operating under a particular spectral set. For example, midday spectra are all quite similar, such that a subset of them become grouped together to create a single proxy spectrum (furthest to the upper-right in Fig. 4b) which represents 17.5% of the total daylight time and 29.7% of the incident solar energy.

The four proxy spectra furthest to the upper right in Fig. 4b represent midday spectra. They lie near the current-matched line and account for nearly half of the daylit time. The lower irradiance (morning, evening and cloudy) spectra encircled toward the lower left represent 27% of the daylit time. (Times corresponding to each spectrum are shown in Fig. S5.†)

The total incident energy (irradiance *x* time) for each spectrum is provided next to each point in Fig. 4b. More than 75% of the total incident solar energy is associated with the four midday spectra furthest toward the upper right. In contrast, the encircled cluster of low-irradiance spectra near the origin accounts for less than 5% of the incident energy. Therefore, any EHE calculation will be dominated by the midday spectra and their spectral variation.

Fig. 5a shows EHE results for this CM tandem under the proxy spectral set. For comparison, the conversion efficiency under the AM1.5G spectrum is shown in Fig. 5b. The two plots are qualitatively similar. The main difference is that the EHE is lower than η(AM1.5G), due to temperature and spectral variations. (Once again, in this and the subsequent two examples, all series resistances and optical losses external to the subcells are neglected to clearly illustrate the effects of spectral mismatch and spectral variability.)

For this CM tandem example the 2T cell performs nearly as well as the 4T cell, indicative of near-perfect current-matching between the subcells. Under a single spectrum (*i.e.*, AM1.5G) it is possible to choose cell parameters which give perfect current-matching, for which the subcells in the 2T cell operate at their respective mpps, producing the same power as they would in a 4T configuration. When the spectrum and conditions are varied, the subcells for the 2T configuration cannot always be at their respective mpps, so the 2T EHE will be lower than the 4T EHE (because the 4T subcells are independently loaded and can therefore always operate at their mpps as the spectrum and conditions vary). In Fig. 5a the difference in EHE is quite small (<1%), because the subcells were still fairly current-matched even as the spectra varied (see Fig. 4b) for the chosen location.

Results for 3T devices are shown for two different VM ratios. A 2/1 VM ratio performs better than a 3/2 ratio because the ratio of the subcell V_{mpp} values (listed in Fig. S3†) is closer to 2/1. Because there are string-end losses for VM strings, the string conversion efficiency increases as the string length increases, and the impact of string-end losses is greater for s-type than r-type tandems.[15]

Overall, when the current-matching is nearly perfect, a 2T configuration is typically the best choice, but it does require a pair of optimum bandgaps and a tunnel junction or other ohmic connection between the subcells. If such a connection or bandgap combination is not possible, then a 4T configuration could be considered, but the optical and I^2R losses associated with a 4T configuration would need to be carefully considered and controlled, as a typical 4T (as in Fig. 1) has three contacts requiring a design compromise between optical transparency and lateral conduction, with their associated I^2R and optical losses. If neither a 2T nor a 4T configuration is viable, then a 3T configuration provides an alternative, but the string-end losses and VM ratio need to be considered.

Voltage-matched tandem

A "VM Tandem" example based upon a 4T GaAs/Si tandem[32] is shown in Fig. 6 and 7. The measured EQE is shown in 6a and the modeled diode parameters are listed in Fig. S2b† with resulting *JV* curves shown as red solid lines in Fig. S3.† Once again, the main difference between the plot for annual EHE (Fig. 7a) and the plot for η(AM1.5G) (Fig. 7b) is that the EHE values are lower, most likely due to the temperature difference. However, the basic trends (which guide cell design) are the same.

As always, a 4T configuration with no resistive or optical losses is the best, but a VM string which constrains the VM ratio to 3/2 performs almost as well. This is because a 3/2 ratio nearly matches the ratio of voltages of these two subcells at mpp (1.47 in this case, as listed in the inset of Fig. S3.†) A string which constrains the subcells to a VM ratio of 2/1 is not quite as good, but still performs much better than a string of series-connected 2T tandem cells. As in the CM tandem example, 3T string-end losses are larger for s-type cells than r-type, but are mitigated by increasing the string length.

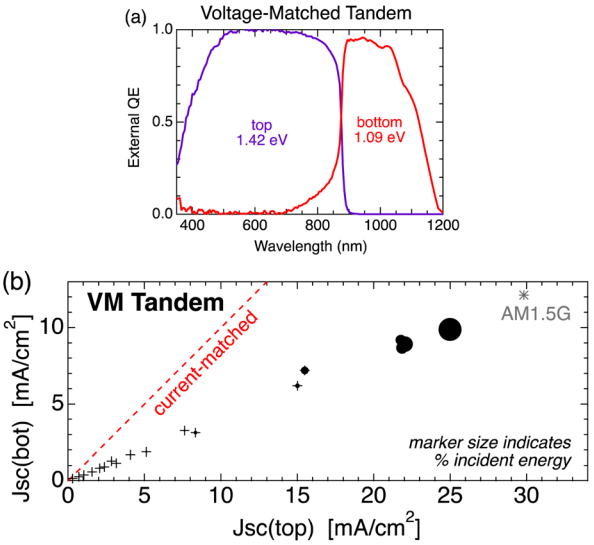

Fig. 6 (a) External quantum efficiency of the voltage-matched tandem example. The *JV* model parameters are listed in Fig. S2b,† but resistive and optical shadow losses are omitted. (b) Photocurrent densities of bottom *versus* top subcells produced by the VM Tandem cell under each spectrum in a set of spectra used for EHE calculations. The size of each point represents the incident energy corresponding to that spectrum, with "+" markers indicating the positions of the smaller points. A grayed point indicating the subcell photocurrent densities under the AM1.5G reference spectrum is included for comparison.

Fig. 6b plots the subcell photocurrent pairs for each spectrum in the proxy set. The subcells are clearly not current matched, which explains the poor performance of the 2T configuration in Fig. 7a and b.

Generic tandem

The last example shows an intermediate case, where the best configuration isn't immediately clear from the cell level data. This "Generic Tandem" example, shown in Fig. 8 and 9, is based upon an s-type 3T GaInP/GaAs tandem cell that we have

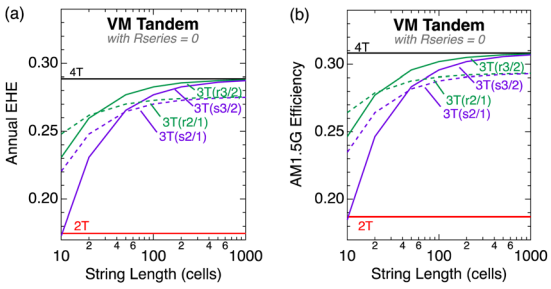

Fig. 7 Cell performance results for a representative voltage-matched (VM) tandem using parameters from Fig. 6. (a) Energy-harvesting efficiency and (b) conversion efficiency under the AM1.5G spectrum for 2T, 3T, and 4T tandems. The 3T curves have been labeled "r *m*/*n*" and "s *m*/*n*", to indicate r- and s-type, respectively, with two representative voltage-matching ratios *m*/*n* of 2/1 and 3/2. Note: All series resistances and optical transmission losses have been set to zero to clearly delineate other effects.

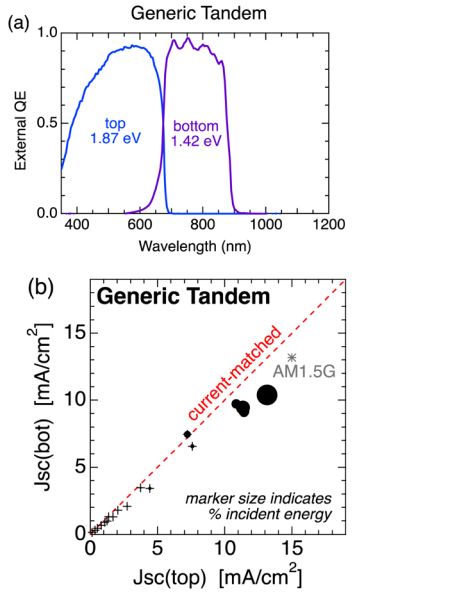

Fig. 8 (a) External quantum efficiency of a generic tandem example (s-type GaInP/GaAs)[23] where the best configuration is not immediately apparent from sub-cell data. The *JV* model parameters are listed in Fig. S2c,† but resistive and optical shadow losses are omitted. (b) Photocurrent densities of bottom *versus* top subcells produced by the generic tandem cell under each spectrum in a set of spectra used for EHE calculations. The size of each point represents the incident energy corresponding to that spectrum, with "+" markers indicating the positions of the smaller points. A grayed point indicating the subcell photocurrent densities under the AM1.5G reference spectrum is included for comparison.

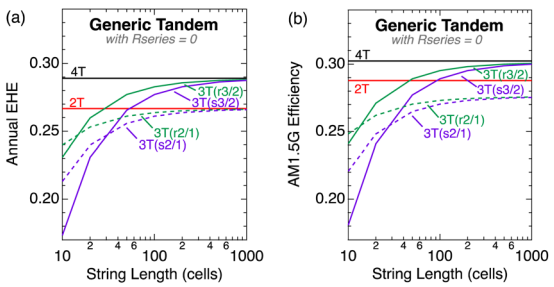

Fig. 9 Cell performance results for a representative "Generic" tandem (non-optimized GaInP/GaAs) using parameters from Fig. 8, intended to illustrate a case in which good performance could be achieved all three configurations (2T, 3T, and 4T). (a) Energy-harvesting efficiency and (b) conversion efficiency under the AM1.5G. The 3T curves have been labeled "r *m*/*n*" and "s *m*/*n*", to indicate r- and s-type, respectively, with two representative voltage-matching ratios *m*/*n* of 2/1 and 3/2. Note: All series resistances and optical transmission losses have been set to zero to clearly delineate other effects. Also, in this paper the term "Generic Tandem" simply refers to an intermediate case which does not heavily favor a 2T, 3T, or 4T design, and is not intended to be representative of all possible scenarios.

previously reported.[23] (The EQE and diode parameters are provided in Fig. 8b and S2c,† respectively.) In this case, all three cell configurations (2T, 3T, and 4T) perform reasonably well. The gap between the 2T and 4T performance is smaller than it was for the VM tandem, but wider than it was for the CM tandem. This is consistent with the data in Fig. 9a showing that current-matching is better for this cell than it was for the VM tandem example, but slightly worse than it was for the CM tandem example.

This example serves to illustrate the difference between current-mismatch and spectral variability. Without the current-mismatch information contained in Fig. 8b, it is impossible to know how much of the performance difference between the 2T and 4T configurations is due to spectral variability, and misconceptions can arise if all the difference is attributed to spectral variability. Using the information contained in Fig. 8b, it is clear that the current mismatch for this example could be reduced by adjusting the design of the cell (*i.e.*, by changing the top-cell bandgap or thickness). If this is done the difference between a 2T and 4T configuration can be decreased until only a small difference due to spectral variability remains.

A 3T tandem in a long 3/2 VM string performs nearly as well as the 4T tandem, because it is a good match to the ratio of subcell voltages when they are operated at their respective mpp (1.44, as listed in Fig. S3†). A 2/1 VM string also works well (and is less complex to string) but is further from the optimal VM ratio. Once again, VM string-end losses are smaller for r-type cells and become negligible for long strings.

Resistive losses

The prior sections of this paper used examples in which all cell resistances were set to zero to focus on other considerations. However, any downselect between 2T, 3T, and 4T configurations must also consider electrical and optical losses, and these losses are typically different for the different configurations. Given the myriad ways that tandem cells can be constructed, these losses can vary over a wide range, but it is still instructive to examine some representative values.

Fig. 10 illustrates how representative resistive losses affect the performance of the different tandem cell designs. The generic tandem cell (described in Fig. 8 and S2c†) is again used for this example, with the VM = 2/1 3T curves omitted to reduce visual clutter.

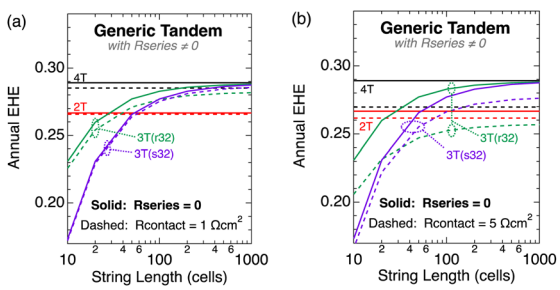

Fig. 10 Energy-harvesting efficiency results for our generic tandem example (non-optimized GaInP/GaAs) recalculated with representative resistance results included. See text for a description of $R_{contact}$. The resistance values in (b) are 5 times larger than the resistance values in (a). Note: Optical transmission losses have been set to zero to clearly delineate other effects, and 3T (2/1) devices have been omitted to reduce overlapping data.

In Fig. 10a, the resistance for the bottom contact of the bottom subcell in all configurations is assumed to be negligible, and all other contacts have been set to an "$R_{contact}$" value of 1 Ω cm^2. Thus, $R_{2T} = 1\ \Omega\ cm^2$ for the 2T case, and $R_T = R_Z = 1\ \Omega\ cm^2$ and $R_R = 0$ for the 3T case. For the 4T case, $R_{top} = 2\ \Omega\ cm^2$, and $R_{bot} = 1\ \Omega\ cm^2$. In Fig. 10b $R_{contact} = 5\ \Omega\ cm^2$ so all resistivities are 5 times larger. These resistive values were chosen primarily for illustrative purposes, but also to provide some guidance for what a maximum tolerable resistivity is likely to be.

As expected for this choice of resistivities, the I^2R losses are larger for the 4T tandem than for the 2T tandem. Although situational, this will typically be the case for actual cases because a 4T tandem has more contacts requiring lateral conduction. In cases where the performance difference between 2T and 4T is small (*i.e.* the CM tandem example in Fig. 5), the 2T performance can exceed the 4T performance when these resistive losses are included, offsetting the 2T tandem's greater spectral sensitivity.

The I^2R losses for 3T tandems are a little more complicated. This is because the current I_Z through the Z contact is always larger for an r-type 3T cell, because it collects the sum of the two subcell currents (see Fig. 2). For an s-type 3T cell, the subcells have the same polarity as a series-connected 2T, so I_Z is the difference between the two currents. This explains why the 3T I^2R losses in Fig. 10 are smaller for s-type cells than for r-type cells. Even without including optical losses (discussed next), this enables the s-type 3T configuration in these examples to outperform the 4T configuration for long strings.

Another subtlety of 3T cells is that a VM constraint can cause the operating current of one or both of the subcells to be larger than it would be for a CM tandem. This explains why the I^2R losses can be greater for an s-type 3T than for a 2T (as in Fig. 10b). However, this effect depends upon the VM ratio, so each case needs to be considered separately and not over-generalized.

Optical losses

All configurations must provide for current collection and optical transmission at the top surface, with some associated optical loss. Typically, for well-designed cells, these optical losses will be small and similar for all designs. However, the light transmission from the top cell to the bottom cell can be quite different for 2T, 3T, and 4T designs.

The 2T and 3T configurations can be grown monolithically, or otherwise fabricated with minimal light loss between the subcells using wafer bonding.[33] In contrast, a 4T tandem must include a dielectric or some other spacer layer for electrical insulation between the subcells. This can introduce an optical loss due to optical index mismatches between this dielectric and the adjacent subcell materials, though in some cases there may also be an opportunity to improve the performance of the top junction by using photon recycling to enhance internal luminescence.[34,35]

In addition, lateral conduction layers and/or grids must be provided to extract current from between the subcells, and this can create additional optical losses due to shadowing and/or free-carrier absorption. However, lower shadow losses are accessible through alignment,[36] subwavelength contacts,[37,38] or by adjusting the TCO used.[39]

Because optical losses are so heavily dependent upon the details of the 4T cell design, we shall consider next the impact of a hypothetical 10% optical transmission loss as a round number purely for illustrative purposes, with the understanding that this value will likely be lower for a well-designed cell. The impact of such an optical loss on a 4T cell can be quickly estimated by knowing the relative power production of the two subcells, because this optical loss only affects the bottom cell.

To understand the implications of this hypothetical optical loss, we can use the "Current-Matched Tandem" in Fig. 5 as an example. In this case, the bottom cell produces approximately half the power of the top cell (1/3 of the total tandem cell power), so reducing the bottom cell light by 10% will reduce the tandem cell power by ~3.3% (relative). This reduces the 4T-tandem EHE from ~26% to ~25%, which is below the 2T-tandem EHE. Although this example is somewhat arbitrary, it illustrates how a 2T device can outperform a 4T device if optical losses are greater for the 4T device. If the same 10% bottom-cell optical loss is applied to the 4T tandem in the "Voltage-Matched Tandem" and "Generic Tandem" examples in Fig. 7 and 9, respectively, the 3T-tandem EHE will similarly be greater than the 4T-tandem EHE.

More detailed calculations would need to consider all of the details of a specific situation, but the optical losses, if not addressed, will typically be largest for a 4T configuration, and this needs to be considered when comparing and tandems with 2T, 3T, and 4T configurations.

Conclusions

This study uses representative examples to illustrate the design considerations associated with 2T, 3T, and 4T tandem cells by modeling both their EHE performance for a set of spectra based on real-world data, and their efficiency under the standard AM1.5G spectrum.

In these comparisons, an idealized 4T tandem with no resistive or optical losses serves as an upper limit for performance. When evaluating actual performance, however, it is important to include these losses because they are typically larger for 4T cells than for 2T and 3T tandems. While not considered in this analysis, 4T cells must also be designed to operate such that the top and bottom cells are electrically isolated, which may introduce additional optical losses and series resistances.

Series-connected 2T tandem cells are more sensitive to spectral variation because the currents passing through the two subcells are constrained to be equal. When the component subcells are "current-matched" the J_{sc} values for both subcells are equal, enabling each subcell to operate at its maximum power point. In outdoor operation, however, the incident spectrum constantly changes, which in turn changes the J_{sc}(top) and J_{sc}(bot). To visualize this, it is helpful to plot the [J_{sc}(top), J_{sc}(bot)] pairs for each spectrum for a given set of outdoor spectra, along with a line indicating the current-matched

condition [J_{sc}(top) = J_{sc}(bot)]. The proximity of the J_{sc} pairs to this line provides useful information about current mismatch and spectral variation, which helps guide design choices.

The performance of VM strings fabricated from 3T tandems is affected by several design choices, and these are most easily visualized by plotting performance as a function of string length for the VM ratios of interest. This facilitates the understanding of the inherent string-end losses for both s-type and r-type 3T tandems. In many cases, if VM 3T strings are sufficiently long, they can outperform 2T tandems in terms of both AM1.5G efficiency and EHE.

In this modeling study, all of the above were initially done with series resistances set to zero. This is helpful because an idealized 4T tandem serves as a very useful benchmark for the upper limit of performance. Once all other losses are understood, then realistic resistive and optical coupling losses should be included for a comprehensive comparison of candidate 2T, 3T, and 4T designs.

In agreement with all prior studies, these methods illustrate the excellent performance of idealized 4T tandem cells and current-matched 2T tandem cells. Adding full string-level analysis shows that 3T tandems can become the preferred choice when subcells are not current-matched or when the optical and resistive losses required to fabricate 4T tandems are substantial. For the location chosen for this study, similar trends are seen for both the energy-harvesting efficiency under a set of spectra, and power-conversion efficiency under the AM1.5G spectrum, illustrating the utility of the AM1.5G spectrum for many design decisions. This analysis can easily be extended to different locations with different climates, and different subcell materials, making this a valuable approach to compare all types of tandem cells.

Author contributions

B. M. – conceptualization, methodology, investigation, writing – original draft. J. G. – methodology, software, data curation, writing – review and editing, J. B. – methodology, software writing – review and editing. E. W. – conceptualization, writing – review and editing, supervision, project administration, funding acquisition.

Conflicts of interest

There are no conflicts to declare.

Acknowledgements

This work was supported by the U.S. Department of Energy under Contract No. DE-AC36-08GO28308 with Alliance for Sustainable Energy, LLC, the Manager and Operator of the National Renewable Energy Laboratory. Funding provided by U.S. Department of Energy Efficiency and Renewable Energy Solar Energy Technologies Office under Agreement Number 34911 and 38266. The U.S. Government retains and the publisher, by accepting the article for publication, acknowledges that the U.S. Government retains a nonexclusive, paid up, irrevocable, worldwide license to publish or reproduce the published form of this work, or allow others to do so, for U.S. Government purposes. The authors would like to acknowledge Adele Tamboli for technical contributions and project leadership; Waldo Olavarría for cell growth; Michelle Young, Talysa Klein, Kaitlyn VanSant and Riley Whitehead for cell fabrication; José Ripalda for supplying the spectral set used in this study; and Robert Witteck for helpful discussions.

Notes and references

1 S. E. Sofia, H. Wang, A. Bruno, J. L. Cruz-Campa, T. Buonassisi and I. M. Peters, *Sustainable Energy Fuels*, 2020, **4**, 852–862.
2 F. Martinho, *Energy Environ. Sci.*, 2021, **14**, 3840–3871.
3 K. T. VanSant, A. C. Tamboli and E. L. Warren, *Joule*, 2021, **5**, 514–518.
4 Y. Gao, R. Lin, K. Xiao, X. Luo, J. Wen, X. Yue and H. Tan, *Joule*, 2022, S2542435122003014.
5 A. Al-Ashouri, E. Köhnen, B. Li, A. Magomedov, H. Hempel, P. Caprioglio, J. A. Márquez, A. B. Morales Vilches, E. Kasparavicius, J. A. Smith, N. Phung, D. Menzel, M. Grischek, L. Kegelmann, D. Skroblin, C. Gollwitzer, T. Malinauskas, M. Jošt, G. Matič, B. Rech, R. Schlatmann, M. Topič, L. Korte, A. Abate, B. Stannowski, D. Neher, M. Stolterfoht, T. Unold, V. Getautis and S. Albrecht, *Science*, 2020, **370**, 1300–1309.
6 R. M. France, J. F. Geisz, T. Song, W. Olavarria, M. Young, A. Kibbler and M. A. Steiner, *Joule*, 2022, **6**, 1121–1135.
7 P. Tockhorn, P. Wagner, L. Kegelmann, J.-C. Stang, M. Mews, S. Albrecht and L. Korte, *ACS Appl. Energy Mater.*, 2020, 1381–1392.
8 M. Schnabel, H. Schulte-Huxel, M. Rienäcker, E. L. Warren, P. F. Ndione, B. Nemeth, T. R. Klein, M. F. A. M. van Hest, J. F. Geisz, R. Peibst, P. Stradins and A. C. Tamboli, *Sustainable Energy Fuels*, 2020, **4**, 549–558.
9 T. Tayagaki, K. Makita, T. Tachibana, H. Mizuno, R. Oshima, H. Takato and T. Sugaya, *IEEE J. Photovoltaics*, 2019, 1–5.
10 F. Gota, M. Langenhorst, R. Schmager, J. Lehr and U. W. Paetzold, *Joule*, 2020, **4**, 2387–2403.
11 E. L. Warren, M. G. Deceglie, M. Rienäcker, R. Peibst, A. C. Tamboli and P. Stradins, *Sustainable Energy Fuels*, 2018, **2**, 1141–1147.
12 J. Lehr, M. Langenhorst, R. Schmager, F. Gota, S. Kirner, U. Lemmer, B. S. Richards, C. Case and U. W. Paetzold, *Sol. Energy Mater. Sol. Cells*, 2020, **208**, 110367.
13 M. T. Hörantner and H. J. Snaith, *Energy Environ. Sci.*, 2017, **10**, 1983–1993.
14 H. Schulte-Huxel, T. J. Silverman, M. G. Deceglie, D. J. Friedman and A. C. Tamboli, *IEEE J. Photovoltaics*, 2018, **8**, 1376–1383.
15 W. E. McMahon, H. Schulte-Huxel, J. Buencuerpo, J. F. Geisz, M. R. Young, T. R. Klein, A. C. Tamboli and E. L. Warren, *IEEE J. Photovoltaics*, 2021, **11**, 1078–1086.
16 S. E. Sofia, N. Sahraei, J. P. Mailoa, T. Buonassisi and I. M. Peters, *IEEE J. Photovoltaics*, 2017, **7**, 934–940.

17 I. J. Park, J. H. Park, S. G. Ji, M.-A. Park, J. H. Jang and J. Y. Kim, *Joule*, 2019, **3**, 807–818.
18 R. Santbergen, R. Mishima, T. Meguro, M. Hino, H. Uzu, J. Blanker, K. Yamamoto and M. Zeman, *Opt. Express*, 2016, **24**, A1288–A1299.
19 D. A. Jacobs, M. Langenhorst, F. Sahli, B. S. Richards, T. P. White, C. Ballif, K. R. Catchpole and U. W. Paetzold, *J. Phys. Chem. Lett.*, 2019, **10**, 3159–3170.
20 M. Spence, R. Hammond, A. Pockett, Z. Wei, A. Johnson, T. Watson and M. J. Carnie, *ACS Appl. Energy Mater.*, 2022, **5**, 5974–5982.
21 T. Feeney, I. M. Hossain, S. Gharibzadeh, F. Gota, R. Singh, P. Fassl, A. Mertens, A. Farag, J.-P. Becker, S. Paetel, E. Ahlswede and U. W. Paetzold, Four-Terminal Perovskite/Copper Indium Gallium Selenide Tandem Solar Cells: Unveiling the Path to >27% in Power Conversion Efficiency, *Sol. RRL*, 2200662, DOI: **10.1002/solr.202200662**.
22 J. F. Geisz, M. A. Steiner, I. Garcia, R. M. France, W. E. McMahon, C. R. Osterwald and D. J. Friedman, *IEEE J. Photovoltaics*, 2015, **5**, 1827–1839.
23 J. F. Geisz, W. E. McMahon, J. Buencuerpo, M. S. Young, M. Rienäcker, A. C. Tamboli and E. L. Warren, *Cell Rep. Phys. Sci.*, 2021, **2**, 100677.
24 J. M. Ripalda and J. Buencuerpo, *Tandems*, **github.com/ripalda/tandems**.
25 D. J. Friedman, J. M. Olson and S. R. Kurtz, in *Handbook of Photovoltaic Science and Engineering*, ed. A. Luque and S. Hegedus, Wiley, Chichester UK, 2nd edn, 2011, pp. 314–364.
26 E. Köhnen, M. Jošt, A. B. Morales-Vilches, P. Tockhorn, A. Al-Ashouri, B. Macco, L. Kegelmann, L. Korte, B. Rech, R. Schlatmann, B. Stannowski and S. Albrecht, *Sustainable Energy Fuels*, 2019, **3**, 1995–2005.
27 W. E. McMahon, K. E. Emery, D. J. Friedman, L. Ottoson, M. S. Young, J. S. Ward, C. M. Kramer, A. Duda and S. Kurtz, *Prog. Photovoltaics*, 2008, **16**, 213–224.
28 J. M. Ripalda, D. Chemisana, J. M. Llorens and I. Garcia, *iScience*, 2020, **23**, 101634.
29 E. L. Warren, W. E. McMahon, M. Rienäcker, K. T. VanSant, R. C. Whitehead, R. Peibst and A. C. Tamboli, *ACS Energy Lett.*, 2020, **5**, 1233–1242.
30 J. M. Ripalda, J. Buencuerpo and I. García, *Nat. Commun.*, 2018, **9**, 5126.
31 D. L. King, W. E. Boyson and J. A. Kratochvill, *Photovoltaic Array Performance Model*, Sandia National Laboratories, Sandia National Laboratories, 2004.
32 K. T. VanSant, E. L. Warren, J. F. Geisz, T. R. Klein, S. Johnston, W. E. McMahon, H. Schulte-Huxel, M. Rienacker, R. Peibst and A. C Tamboli, *iScience*, 2022, **25**, 104950.
33 R. M. Patrick Schygulla, *Prog. Photovoltaics*, 2022, **30**, 689.
34 R. C. Whitehead, K. T. VanSant, E. L. Warren, J. Buencuerpo, M. Rienäcker, R. Peibst, J. F. Geisz and A. C. Tamboli, *Appl. Phys. Lett.*, 2021, **118**, 183902.
35 V. Ganapati, C.-S. Ho and E. Yablonovitch, *IEEE J. Photovoltaics*, 2015, **5**, 410–417.
36 S. Essig, C. Allebé, T. Remo, J. F. Geisz, M. A. Steiner, K. Horowitz, L. Barraud, J. S. Ward, M. Schnabel, A. Descoeudres, D. L. Young, M. Woodhouse, M. Despeisse, C. Ballif and A. Tamboli, *Nat. Energy*, 2017, **2**, 17144.
37 E. San Román, A. Vitrey, J. Buencuerpo, I. Prieto, J. M. Llorens, A. García-Martín, B. Alén, A. Chaudhuri, A. Neumann, S. R. J. Brueck and J. M. Ripalda, *Sci. Rep.*, 2016, **6**, 28669.
38 C. P. Muzzillo, *Sol. Energy Mater. Sol. Cells*, 2017, **169**, 68–77.
39 M. Morales-Masis, S. De Wolf, R. Woods-Robinson, J. W. Ager and C. Ballif, *Adv. Electron. Mater.*, 2017, **3**, 1600529.